ACS APPLIED MATERIALS & INTERFACES

www.acsami.org

Research Article

Ultrafast Photocurrent Response and High Detectivity in Two-Dimensional $MoSe_2$-based Heterojunctions

Christian D. Ornelas, Arthur Bowman, Thayer S. Walmsley, Tianjiao Wang, Kraig Andrews, Zhixian Zhou, and Ya-Qiong Xu*

Cite This: *ACS Appl. Mater. Interfaces* 2020, 12, 46476–46482

Read Online

ACCESS | Metrics & More | Article Recommendations | Supporting Information

ABSTRACT: Two-dimensional (2D) transition metal dichalcogenide (TMDC) materials have garnered great attention on account of their novel properties and potential to advance modern technology. Recent studies have demonstrated that TMDCs can be utilized to create high-performing heterostructures with combined functionality of the individual layers and new phenomena at these interfaces. Here, we report an ultrafast photoresponse within $MoSe_2$-based heterostructures in which heavily p-doped WSe_2 and MoS_2 flakes share an undoped $MoSe_2$ channel, allowing us to directly compare the optoelectronic properties of $MoSe_2$-based heterojunctions with different 2D materials. Strong photocurrent signals have been observed in both $MoSe_2$–WSe_2 and $MoSe_2$–MoS_2 heterojunctions with a photoresponse time constant of ~16 μs, surmounting previous $MoSe_2$-based devices by three orders of magnitude. Further studies have shown that the fast response is independent of the integrated 2D materials (WSe_2 or MoS_2) but is likely attributed to the high carrier mobility of 260 $cm^2\ V^{-1}\ s^{-1}$ in the undoped $MoSe_2$ channel as well as the greatly reduced Schottky barriers and near absence of interface states at $MoSe_2$–WSe_2/MoS_2 heterojunctions, which lead to reduced carrier transit time and thus short photocurrent response time. Lastly, a high detectivity on the order of $\sim 10^{14}$ Jones has been achieved in $MoSe_2$-based heterojunctions, which supersedes current industry standards. These fundamental studies not only shed light on photocurrent generation mechanisms in $MoSe_2$-based heterojunctions but also open up new avenues for engineering future high-performance 2D optoelectronic devices.

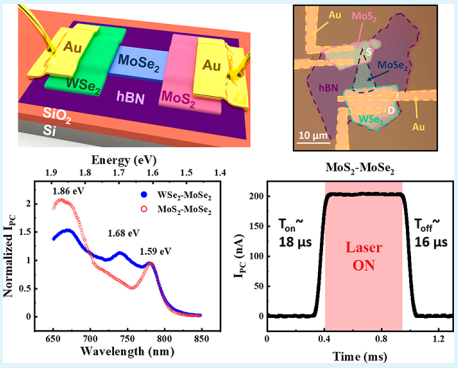

KEYWORDS: *heterojunction, 2D Materials, $MoSe_2$, TMDCs, photocurrent*

INTRODUCTION

Two-dimensional (2D) van der Waals (vdW) materials have received considerable attention due to their novel electrical, optical, and mechanical properties as well as the ease of heterostructure fabrication of lattice mismatched materials without strain.[1] In particular, transition metal dichalcogenides (TMDCs) have established themselves as an attractive class of 2D materials as they typically feature sizeable band gaps, strong light–matter interactions, and broad spectral responses.[2] These characteristics naturally facilitate the incorporation of TMDCs into electronic and optoelectronic devices, such as field-effect transistors (FETs),[3−5] photodetectors,[6] photovoltaic cells,[7,8] and many other applications.[9] While some device improvements are achieved through the use of different TMDC channels,[10−12] other works suggest that 2D heterostructures will also enhance device performance.[13−16] Therefore, substantial efforts have been expended in understanding the underlying mechanisms within TMDC heterostructures[17−22] and their commercial synthesis.[23−26] For example, it has been shown that heterostructures consisting of different atomically thin materials like black phosphorus, graphene, and TMDCs can result in devices with improved optoelectronic properties, such as increased mobility and reduced response times while foregoing thermal stability in the former examples.[14,27−29] Moreover, heterostructures formed between heavily doped TMDCs and undoped TMDCs display similar enhancements whilst further reducing Schottky barrier heights, resulting in low-resistance ohmic contacts.[30] Such improvements are imperative to attain high-performance optoelectronic devices which allow for the ultrafast movement of information, a highly sought after property of commercial and academic endeavors alike.[31]

Recently, $MoSe_2$-based devices have become more prominent as their weakly bound excitons result in intrinsically faster response times.[32] $MoSe_2$ holds properties indicative of its value in optoelectronic applications, such as a sizable direct band gap of ~1.6 eV,[33,34] high optical absorption,[7] and carrier mobility reaching 100 $cm^2\ V^{-1}\ s^{-1}$.[35] Despite three-dimensional $MoSe_2$-based heterostructures featuring exceedingly fast response

Received: July 5, 2020
Accepted: September 1, 2020
Published: September 1, 2020

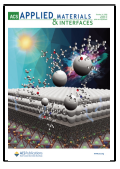

https://dx.doi.org/10.1021/acsami.0c12155
ACS Appl. Mater. Interfaces 2020, 12, 46476–46482

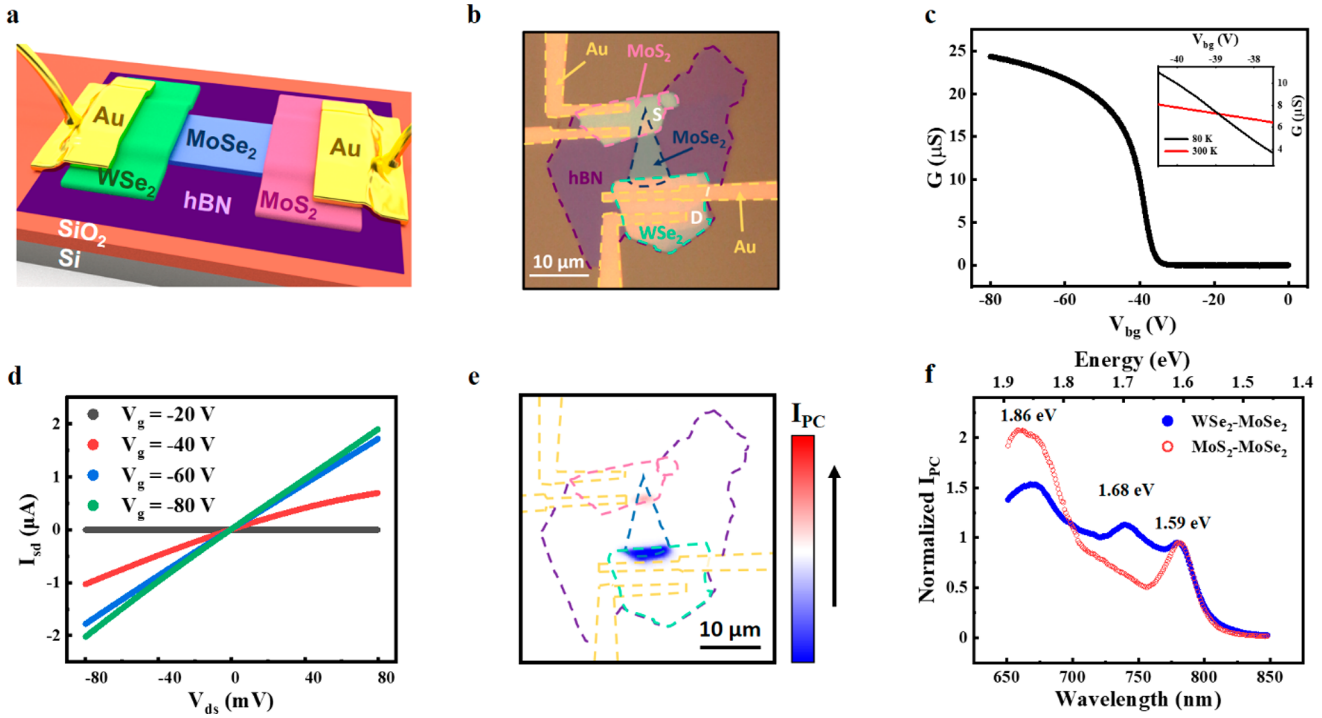

Figure 1. (a) Schematic illustrating the composition of a $MoSe_2$-based heterostructure. (b) Optical micrograph of a typical device with dashed outlines to indicate the material layout. S and D correspond to source and drain contacts, respectively. (c) Transport characteristics of a device with respect to the back-gate voltage. Inset: the linear region for mobility calculation at 80 K (black) and room temperature (red), respectively. (d) I_{ds}–V_{ds} characteristics at various back-gate voltages at ~80 K. (e) Scanning photocurrent image of the device under −30 mV bias. (f) Normalized wavelength dependence of the photocurrent signals under −30 mV ($MoSe_2$–WSe_2) and 0 V ($MoSe_2$–MoS_2) bias voltages, respectively.

times,[36] response times of 2D $MoSe_2$-based devices are on the scale of milliseconds,[35,37−39] which are significantly slower than those of commercial semiconductors.[40] Therefore, it is important to investigate $MoSe_2$-based heterostructures with inherited unique properties from $MoSe_2$ plus the fast photoresponse.

In this work, we report the ultrafast photoresponse in $MoSe_2$–WSe_2 and $MoSe_2$–MoS_2 heterojunctions, where heavily p-doped MoS_2 and WSe_2 flakes are bridged by an undoped $MoSe_2$ channel. The fast rise and decay time constants (as low as ~16 μs) have been achieved in both $MoSe_2$–WSe_2 and $MoSe_2$–MoS_2 heterojunctions. Further studies have shown that the fast photoresponse likely results from the high carrier mobility (260 $cm^2\ V^{-1}s^{-1}$) as well as negligible Schottky barriers and near absence of interface states at $MoSe_2$–WSe_2/MoS_2 heterojunctions, which are expected to reduce the carrier transit time and thus the photoresponse time. Moreover, a detectivity of $\sim 10^{14}$ Jones has been observed in $MoSe_2$-based heterojunctions, which are higher than commercial Si- and InGaAs-based photodetectors. Our experimental results offer a way to build ultrafast 2D heterojunctions, opening a door for engineering future high-performance 2D optoelectronics.

EXPERIMENTAL SECTION

Device Fabrication. $MoSe_2$, heavily p-doped WSe_2 ($Nb_{0.005}W_{0.995}Se_2$), heavily p-doped WSe_2 ($Nb_{0.005}M_{0.995}S_2$), and hBN flakes were mechanically exfoliated from bulk crystals and transferred via a dry transfer method to a silicon substrate with 280 nm of thermally grown SiO_2. The thickness of each material was identified by noncontact mode atomic force microscopy (Park-System XE-70). Electron beam lithography and subsequent deposition of Au/Ti were used to form metal electrodes for the heavily p-doped TMDCs.

Electrical and Optoelectronic Characterization. All experiments were performed in a Janis ST-500 microscopy cryostat in a high vacuum environment (~10^{-6} Torr). Current signals were collected via a DL instrument 1211 current preamplifier. Scanning photocurrent measurements were executed using an Olympus BX51WI microscope. A linearly polarized continuous wave laser beam (NKT Photonics SuperK Supercontinuum Laser) was expanded and focused with a 40x objective (N.A. = 0.6) into a diffraction-limited spot (~1 μm) and scanned over the device by a piezo-controlled mirror with nanometer-scale spatial resolution.

RESULTS AND DISCUSSION

Figure 1a depicts a schematic diagram of the $MoSe_2$ heterostructure that consists of an undoped $MoSe_2$ channel with two asymmetric contacts of heavily p-doped WSe_2 and MoS_2 flakes, respectively, which are connected to Au/Ti electrodes. $MoSe_2$ has been selected as a channel material, while other TMDCs with distinct band gaps serve as a basis for the choice of contact materials. This not only sheds light on the photocurrent generation mechanisms in TMDC-based heterojunctions but also provides a way to fabricate fast $MoSe_2$ phototransistors. The device is fabricated on top of a thin flake of hBN to provide a clean substrate and thus to avoid charge traps and surface bonds present on SiO_2.[41] An optical image of a typical device is presented in Figure 1b, where different materials are outlined with the following color scheme: Au contacts (yellow), hBN (purple), WSe_2 (green), $MoSe_2$ (blue), and MoS_2 (pink). As shown in Figure S1, the MoS_2 and WSe_2 flakes were ~23 nm and ~16 nm thick, respectively, while the $MoSe_2$ channel and hBN were ~7 nm and ~15 nm, respectively. These materials were mechanically exfoliated

https://dx.doi.org/10.1021/acsami.0c12155
ACS Appl. Mater. Interfaces 2020, 12, 46476−46482

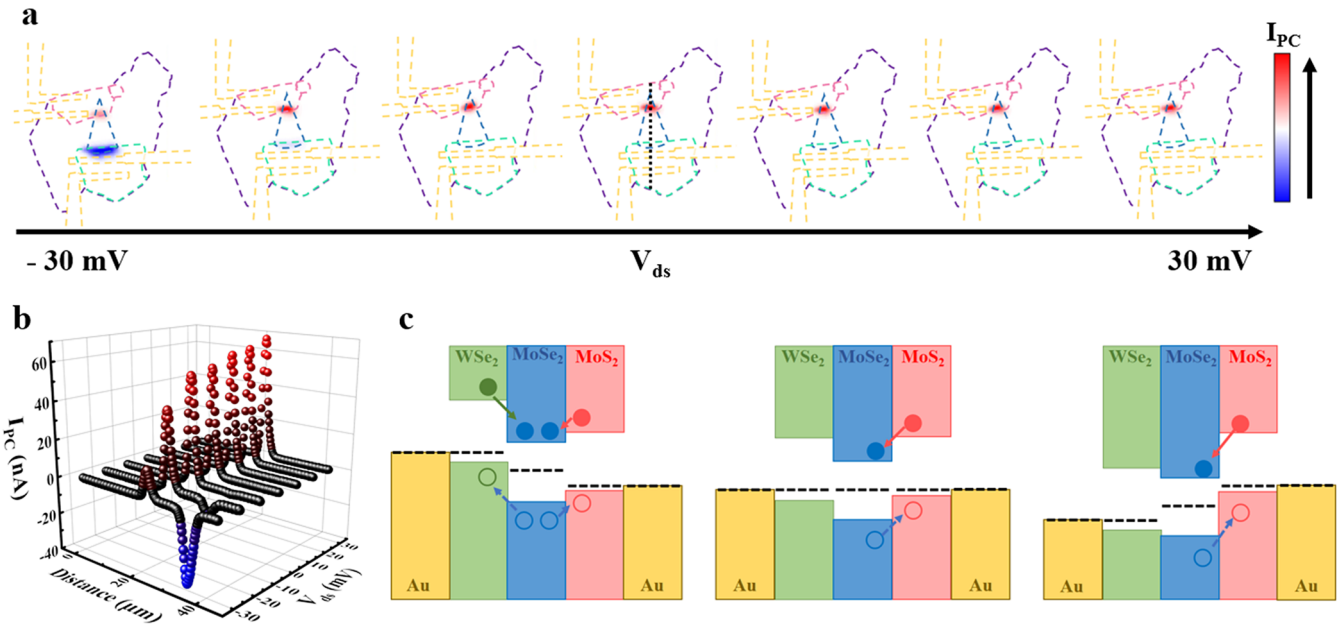

Figure 2. (a) Scanning photocurrent signal under various drain-source bias voltages. (b) Numerical representation of photocurrent under different bias voltages along a single scanline, depicted by a dotted line in (a). (c) Band diagrams for the device under V_{ds} = −30 mV, 0V, and 30 mV, respectively.

from bulk crystals, and their thickness was found via atomic force microscopy (AFM). The undoped $MoSe_2$ and the heavily p-doped TMDC heterojunctions were formed via a dry transfer method. Electron beam lithography and deposition of 50/5 nm Au/Ti were subsequently conducted to form the metal electrodes. A dielectric stack made of 280 nm SiO_2 and a ∼15 nm hBN flake facilitates the application of a back-gate voltage to the device. The electrical and optoelectronic properties of this device were investigated under high vacuum ($\sim 10^{-6}$ Torr) and at a low temperature (80 K) using a Janis ST-500 microscopy cryostat. Figure 1c shows a p-type behavior of the device, which is due to the two heavily p-doped contacts (WSe_2 and MoS_2) that only allow the $MoSe_2$ channel to be turned on under a negative gate voltage. The field-effect hole mobilities are extrapolated as ∼260 $cm^2\ V^{-1}\ s^{-1}$ at 80 K and ∼70 $cm^2\ V^{-1}\ s^{-1}$ at room temperature, respectively, which is higher than previous reports of $MoSe_2$ devices.[35,42−44] Specifically, the expression used to calculate mobility is $\mu_{FET} = (1/C_{bg}) \times (L/W) \times (d\sigma/dV_{bg})$, where C_{bg} is the back-gate capacitance of the 280 nm thick SiO_2 in series with a ∼15 nm hBN flake, L and W are the length and average width of the channel, respectively, and the derivative is the extrapolated slope of the linear portion of the transfer curve. Figure 1d displays linear and symmetric output characteristics of the $MoSe_2$ heterostructure when a wide range of back-gate voltages were applied at 80 K, indicating ohmic behaviors of the device. This suggests that the 2D/2D contacts allow low contact resistance, and the resistances between heavily p-doped TMDCs and external metal electrodes are negligible due to the tunneling effect through an extremely narrow (on the order of nm) depletion region, leading to high hole mobility of our device.[30,34,45]

Next, we explore the optoelectronic properties of the $MoSe_2$ heterostructure using spatially resolved scanning photocurrent measurements. The positions of the photocurrent signals ($I_{PC} = I_{laser} - I_{dark}$) were precisely located by the correlation of the reflection image of the device with its optical image, as depicted by Figure 1e, where the red/blue color represents positive/negative photocurrent. As seen in the aforementioned figure, remarkable photocurrent signals are found at both $MoSe_2$−WSe_2 and $MoSe_2$−MoS_2 heterojunctions. To further investigate the contrasting characteristics of these heterojunctions, the wavelength-dependent photocurrent measurements were conducted with a focused beam. Here, the device was explored under the drain-source bias of −30 mV and zero bias for $MoSe_2$−WSe_2 and $MoSe_2$−MoS_2 heterojunctions, respectively. Figure 1f shows a photocurrent peak at ∼1.59 eV detected in both heterojunctions, which is likely related to the A exciton energy of few-layer $MoSe_2$.[46] This observation indicates that the photocurrent signals mainly result from the optical absorption of the $MoSe_2$ channel under 780 nm illumination. Moreover, a photocurrent peak is observed at ∼1.68 eV in the $MoSe_2$−WSe_2 heterojunction, which is close to the A exciton energy of WSe_2.[22,47] This suggests that the p-doped WSe_2 flake also contributes to the photocurrent generation at the heterojunctions. Interestingly, a maximum photocurrent signal is found at both heterojunctions for wavelengths with energies surrounding ∼1.84 eV, which may be attributed to the B exciton energy of the $MoSe_2$ channel.[48,49] We also know that the A exciton energy of few-layer MoS_2 occurs in this region of the spectrum (1.8 − 1.9 eV).[50,51] Indeed, the photocurrent intensity of the $MoSe_2$−MoS_2 heterojunction is higher than that of the $MoSe_2$−WSe_2 heterojunction under 674 nm illumination, suggesting that the contribution from the optical absorption of the p-doped MoS_2 flake cannot be neglected. Our experimental results indicate that both the undoped $MoSe_2$ and p-doped MoS_2/WSe_2 flakes contribute to the photocurrent generations in these heterojunctions.

To further elucidate the photoresponse generation mechanisms of $MoSe_2$-based heterojunctions, bias-dependent scanning photocurrent measurements were performed by sweeping the drain-source bias voltages from −30 to 30 mV. The resulting photocurrent mappings of the device are depicted in

https://dx.doi.org/10.1021/acsami.0c12155
ACS Appl. Mater. Interfaces 2020, 12, 46476−46482

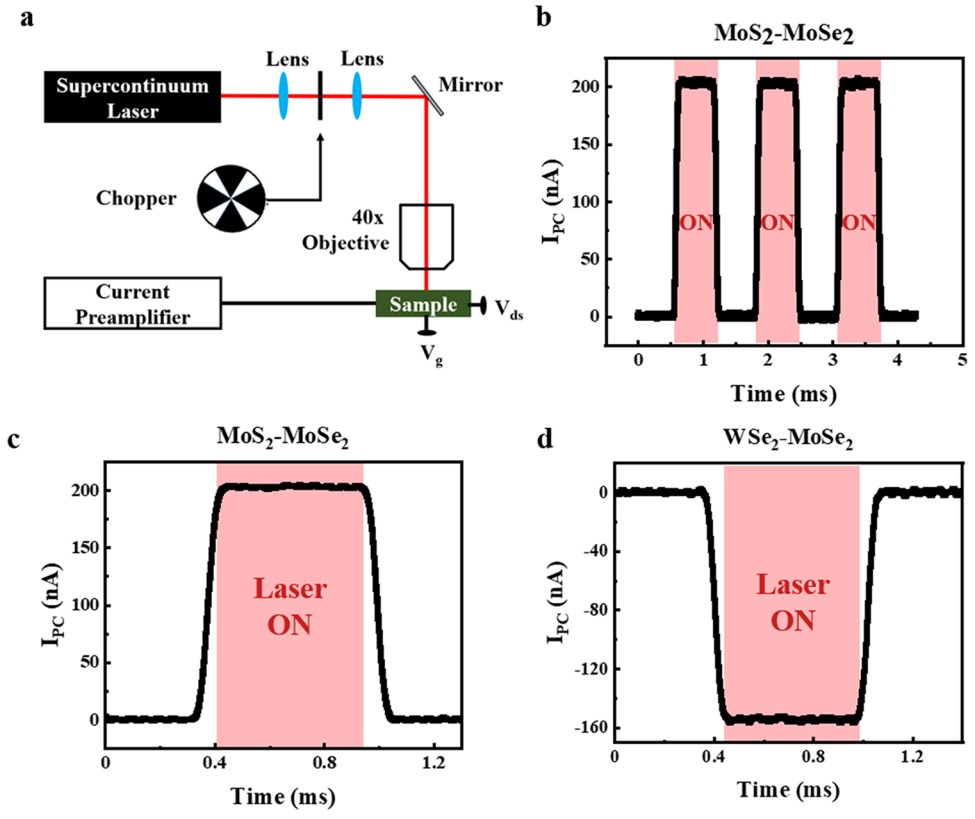

Figure 3. (a) Diagram depicting the experimental setup used to measure time-dependent photocurrent signals. (b) Photocurrent responses as a function of time under 650 nm illumination. The photocurrent signals were collected for the (c) $MoSe_2$−MoS_2 junction under zero bias and the (d) $MoSe_2$−WSe_2 junction with V_{ds} = −30 mV, respectively.

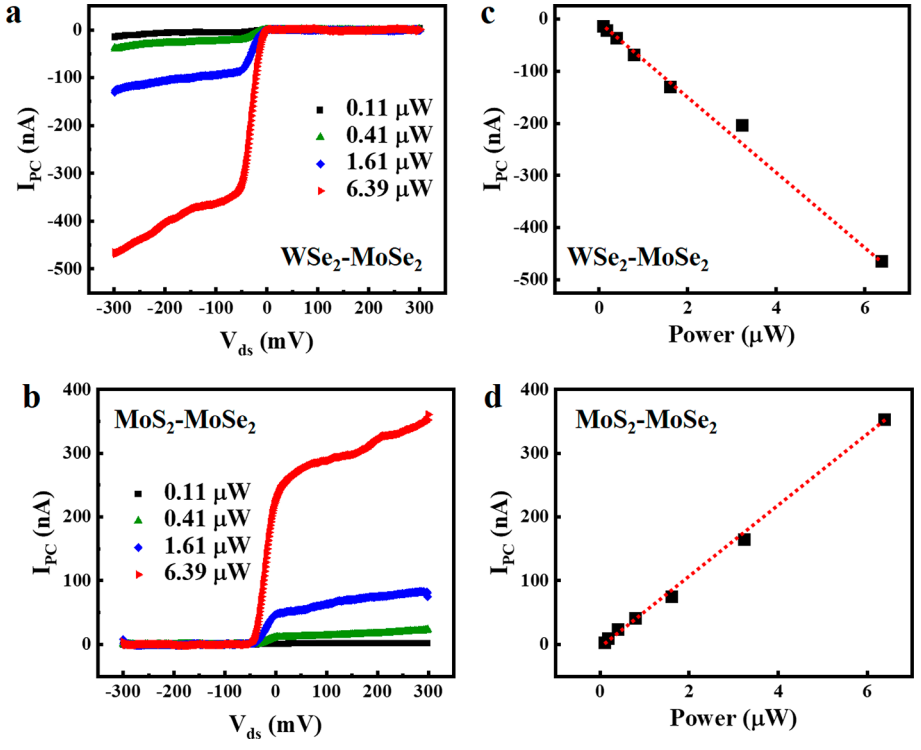

Figure 4. Photocurrent signals as a function of drain-source bias under a zero gate voltage for various values of laser power (λ = 650 nm) on (a) $MoSe_2$−WSe_2 and (b) $MoSe_2$−MoS_2 junctions, respectively. Power dependence of photocurrent responses on (c) $MoSe_2$−WSe_2 and (d) $MoSe_2$−MoS_2 junctions, respectively.

https://dx.doi.org/10.1021/acsami.0c12155
ACS Appl. Mater. Interfaces 2020, 12, 46476−46482

Figure 2a, while quantitative measurements of photocurrent are extracted along the black dotted line and plotted spatially in Figure 2b. Under zero bias, photocurrent responses are primarily observed at the $MoSe_2$−MoS_2 junction, where electron-hole pairs (EHPs) are separated by a band offset between the heavily p-doped MoS_2 and undoped $MoSe_2$ flakes, leading to a current from $MoSe_2$ to MoS_2. The relatively weak photocurrent response at the $MoSe_2$−WSe_2 junction is likely attributed to a smaller band offset between the $MoSe_2$ and WSe_2, suggesting that the p-doping level in the WSe_2 flake is slightly lower than that in the MoS_2 flake. When the bias is increased to 30 mV, the band offset at the $MoSe_2$−MoS_2 junction increases, and consequently, the photocurrent intensity is enhanced. On the other hand, when the device is under a negative bias voltage of −30 mV, negative photocurrent signals begin to appear at the $MoSe_2$−WSe_2 heterojunction, which may result from the increase in the band offset between the undoped $MoSe_2$ and p-doped WSe_2 flakes. Here, the photoexcited holes can flow from $MoSe_2$ to WSe_2 and thus generate negative photocurrent responses at this heterojunction. These behaviors are depicted in Figure 2c and Figure S2.

The temporal response of the device was subsequently explored using an ON/OFF light modulation accomplished by the addition of an optical chopper to the laser path, as shown in Figure 3a. The photocurrent signals can be plotted versus time (Figure 3b), where the rise and decay time constants of the signals are extracted with a single exponential fitting function. Under zero bias, where the $MoSe_2$−MoS_2 heterojunction features sizable photocurrent signals, the rise and decay time constants are ∼18 μs and ∼16 μs (Figure 3c), respectively, which are three orders of magnitude faster than previous 2D $MoSe_2$-based phototransistors[4,10,38,39,52−57] and is comparable with other 2D TMDC phototransistors.[29,58] Interestingly, the rise and decay time constants for the $MoSe_2$−WSe_2 heterojunction under −30 mV bias are ∼ 17 μs (Figure 3d), which are similar to those of the $MoSe_2$−MoS_2 heterojunction. The ultrafast photoresponse in $MoSe_2$-based heterojunctions is likely attributed to their unique 2D/2D heterostructures, where the near absence of interface states at the $MoSe_2$−WSe_2 and $MoSe_2$−MoS_2 van der Waals heterojunctions can significantly reduce charge trapping compared to conventional metal−2D semiconductor junctions, where interface states are almost ubiquitous. (More details are present in the Supporting Information.) In addition, the high mobility of 260 $cm^2\ V^{-1}\ s^{-1}$ in the $MoSe_2$ channel on the hBN substrate and the greatly lowered Schottky barriers at the heterojunction contacts are expected to reduce transit time and thus shorten photoresponse time. Furthermore, the photoexcited carriers can be easily collected by the external metal electrodes through the tunneling effect due to the narrow depletion region between heavily doped TMDCs and metal electrodes.

The performance of the $MoSe_2$ heterostructure device was subsequently assessed when the device is in the OFF state with a negligible dark current of $\sim 10^{-10}$ A. Figure 4a,b shows the photocurrent signals of the $MoSe_2$-based heterojunctions with various laser powers when the drain-source bias voltages are swept from −300 to 300 mV. The photocurrent signals of the $MoSe_2$−WSe_2 junction are negligible for zero and positive bias voltages, while exponentially increasing as the bias changes from zero to approximately −50 mV. As the negative bias further increases beyond −50 mV, the photocurrent signals at the $MoSe_2$−WSe_2 junction increase at a much slower rate. On the other hand, the $MoSe_2$−MoS_2 junction features substantial photocurrent signals even under zero bias, which slowly increase with an increasing positive bias voltage. As the bias changes from zero to negative, the photocurrent signals drop rapidly and nearly diminish at −50 mV. The photocurrent intensity shows a linear dependence on laser power with maximum photoresponsivities of $\sim 140^{-1}$ and ∼60 mA W^{-1} for $MoSe_2$−WSe_2 and $MoSe_2$−MoS_2 junctions (Figure 4c,d), respectively, suggesting that photocurrent generation is directly proportional to absorption of incident photons.[59] Furthermore, the $MoSe_2$-based heterojunctions demonstrate a high specific detectivity on the order of $\sim 10^{14}$ Jones, a value better than state-of-the-art devices frequently used for photodetection.[60]

CONCLUSIONS

In conclusion, we report $MoSe_2$-based heterostructures with a fast photoresponse of as low as ∼16 μs, which is three orders of magnitudes faster than previously reported values for $MoSe_2$-based devices. Moreover, detectivity on the order of $\sim 10^{14}$ Jones has been achieved in our $MoSe_2$-based heterojunctions, greater than current industry standards. Further studies have shown that the ultrafast photoresponse is not dependent on the integrated TMDC materials (either heavily p-doped WSe_2 or MoS_2) in $MoSe_2$-based heterojunctions, but it is likely attributed to the high hole mobility (260 $cm^2\ V^{-1}\ s^{-1}$) and negligible contact resistance at 2D/2D interfaces,[30] which are expected to foster carrier transit time and thus shorten the photocurrent response times. These results suggest that ultrafast performance can be attained within $MoSe_2$-based heterojunctions, providing a way to build future ultrafast 2D optoelectronics.

ASSOCIATED CONTENT

Supporting Information

The Supporting Information is available free of charge at https://pubs.acs.org/doi/10.1021/acsami.0c12155.

Thickness of different materials, energy levels of different materials, and mechanisms for a fast photocurrent response (PDF)

AUTHOR INFORMATION

Corresponding Author

Ya-Qiong Xu − *Department of Physics and Astronomy and Department of Electrical Engineering and Computer Science, Vanderbilt University, Nashville, Tennessee 37235, United States of America*; orcid.org/0000-0003-1423-7458; Email: yaqiong.xu@vanderbilt.edu

Authors

Christian D. Ornelas − *Department of Physics and Astronomy, Vanderbilt University, Nashville, Tennessee 37235, United States of America*

Arthur Bowman − *Department of Physics and Astronomy, Wayne State University, Detroit, Michigan 48201, United States of America*

Thayer S. Walmsley − *Department of Physics and Astronomy, Vanderbilt University, Nashville, Tennessee 37235, United States of America*

Tianjiao Wang − *Department of Electrical Engineering and Computer Science, Vanderbilt University, Nashville, Tennessee 37235, United States*

https://dx.doi.org/10.1021/acsami.0c12155
ACS Appl. Mater. Interfaces 2020, 12, 46476−46482

Kraig Andrews − *Department of Physics and Astronomy, Wayne State University, Detroit, Michigan 48201, United States of America*

Zhixian Zhou − *Department of Physics and Astronomy, Wayne State University, Detroit, Michigan 48201, United States of America;* orcid.org/0000-0002-9228-4260

Complete contact information is available at: https://pubs.acs.org/10.1021/acsami.0c12155

Notes

The authors declare no competing financial interest.

■ ACKNOWLEDGMENTS

This work was supported by the National Science Foundation (ECCS-1810088, CBET-1805924, and DMR-2004445).

■ REFERENCES

(1) Zhang, H. Ultrathin Two-Dimensional Nanomaterials. *ACS Nano* **2015**, *9*, 9451−9469.

(2) Choi, W.; Choudhary, N.; Han, G. H.; Park, J.; Akinwande, D.; Lee, Y. H. Recent Development of Two-Dimensional Transition Metal Dichalcogenides and Their Applications. *Mater. Today* **2017**, 116−130.

(3) Pudasaini, P. R.; Stanford, M. G.; Oyedele, A.; Wong, A. T.; Hoffman, A. N.; Briggs, D. P.; Xiao, K.; Mandrus, D. G.; Ward, T. Z.; Rack, P. D. High Performance Top-Gated Multilayer WSe_2 Field Effect Transistors. *Nanotechnology* **2017**, *28*, 475202.

(4) Radisavljevic, B.; Radenovic, A.; Brivio, J.; Giacometti, V.; Kis, A. Single-Layer MoS_2 Transistors. *Nat. Nanotechnol.* **2011**, *6*, 147−150.

(5) Lin, J.; Zhong, J.; Zhong, S.; Li, H.; Zhang, H.; Chen, W. Modulating Electronic Transport Properties of MoS_2 Field Effect Transistor by Surface Overlayers. *Appl. Phys. Lett.* **2013**, *103*, No. 063109.

(6) Xue, Y.; Zhang, Y.; Liu, Y.; Liu, H.; Song, J.; Sophia, J.; Liu, J.; Xu, Z.; Xu, Q.; Wang, Z.; Zheng, J.; Liu, Y.; Li, S.; Bao, Q. Scalable Production of a Few-Layer MoS_2/WS_2 Vertical Heterojunction Array and Its Application for Photodetectors. *ACS Nano* **2016**, *10*, 573−580.

(7) Bernardi, M.; Palummo, M.; Grossman, J. C. Extraordinary Sunlight Absorption and One Nanometer Thick Photovoltaics Using Two-Dimensional Monolayer Materials. *Nano Lett.* **2013**, *13*, 3664−3670.

(8) Flöry, N.; Jain, A.; Bharadwaj, P.; Parzefall, M.; Taniguchi, T.; Watanabe, K.; Novotny, L. A $WSe_2/MoSe_2$ Heterostructure Photovoltaic Device. *Appl. Phys. Lett.* **2015**, *107*, 123106.

(9) Bhimanapati, G. R.; Lin, Z.; Meunier, V.; Jung, Y.; Cha, J.; Das, S.; Xiao, D.; Son, Y.; Strano, M. S.; Cooper, V. R.; Liang, L.; Louie, S. G.; Ringe, E.; Zhou, W.; Kim, S. S.; Naik, R. R.; Sumpter, B. G.; Terrones, H.; Xia, F.; Wang, Y.; Zhu, J.; Akinwande, D.; Alem, N.; Schuller, J. A.; Schaak, R. E.; Terrones, M.; Robinson, J. A. Recent Advances in Two-Dimensional Materials beyond Graphene. *ACS Nano* **2015**, *9*, 11509−11539.

(10) Lopez-Sanchez, O.; Lembke, D.; Kayci, M.; Radenovic, A.; Kis, A. Ultrasensitive Photodetectors Based on Monolayer MoS_2. *Nat. Nanotechnol.* **2013**, *8*, 497−501.

(11) Choi, W.; Cho, M. Y.; Konar, A.; Lee, J. H.; Cha, G. B.; Hong, S. C.; Kim, S.; Kim, J.; Jena, D.; Joo, J.; Kim, S. High-Detectivity Multilayer MoS_2 Phototransistors with Spectral Response from Ultraviolet to Infrared. *Adv. Mater.* **2012**, *24*, 5832−5836.

(12) Xie, C.; Mak, C.; Tao, X.; Yan, F. Photodetectors Based on Two-Dimensional Layered Materials Beyond Graphene. *Adv. Funct. Mater.* **2017**, *27*, 1603886.

(13) Huo, N.; Kang, J.; Wei, Z.; Li, S.-S.; Li, J.; Wei, S.-H. Novel and Enhanced Optoelectronic Performances of Multilayer MoS_2-WS_2 Heterostructure Transistors. *Adv. Funct. Mater.* **2014**, *24*, 7025−7031.

(14) Ye, L.; Li, H.; Chen, Z.; Xu, J. Near-Infrared Photodetector Based on MoS_2/Black Phosphorus Heterojunction. *ACS Photonics* **2016**, *3*, 692−699.

(15) Georgiou, T.; Jalil, R.; Belle, B. D.; Britnell, L.; Gorbachev, R. V.; Morozov, S. V.; Kim, Y.-J.; Gholinia, A.; Haigh, S. J.; Makarovsky, O.; Eaves, L.; Ponomarenko, L. A.; Geim, A. K.; Novoselov, K. S.; Mishchenko, A. Vertical Field-Effect Transistor Based on Graphene−WS_2 Heterostructures for Flexible and Transparent Electronics. *Nat. Nanotechnol.* **2013**, *8*, 100−103.

(16) Yu, W. J.; Liu, Y.; Zhou, H.; Yin, A.; Li, Z.; Huang, Y.; Duan, X. Highly Efficient Gate-Tunable Photocurrent Generation in Vertical Heterostructures of Layered Materials. *Nat. Nanotechnol.* **2013**, *8*, 952−958.

(17) Ross, J. S.; Rivera, P.; Schaibley, J.; Lee-Wong, E.; Yu, H.; Taniguchi, T.; Watanabe, K.; Yan, J.; Mandrus, D.; Cobden, D.; Yao, W.; Xu, X. Interlayer Exciton Optoelectronics in a 2D Heterostructure p−n Junction. *Nano Lett.* **2017**, *17*, 638−643.

(18) Zhang, N.; Surrente, A.; Baranowski, M.; Maude, D. K.; Gant, P.; Castellanos-Gomez, A.; Plochocka, P. Moiré Intralayer Excitons in a $MoSe_2/MoS_2$ Heterostructure. *Nano Lett.* **2018**, *18*, 7651−7657.

(19) Ben Amara, I.; Ben Salem, E.; Jaziri, S. Optoelectronic Response and Interlayer Exciton Features of MoS_2/WS_2 Van Der Waals Heterostructure within First Principle Calculations and Wannier Mott Model. *Superlattices Microstruct.* **2017**, *109*, 897−904.

(20) Baranowski, M.; Surrente, A.; Klopotowski, L.; Urban, J. M.; Zhang, N.; Maude, D. K.; Wiwatowski, K.; Mackowski, S.; Kung, Y. C.; Dumcenco, D.; Kis, A.; Plochocka, P. Probing the Interlayer Exciton Physics in a MoS_2 /$MoSe_2$ /MoS_2 van Der Waals Heterostructure. *Nano Lett.* **2017**, *17*, 6360−6365.

(21) Rivera, P.; Seyler, K. L.; Yu, H.; Schaibley, J. R.; Yan, J.; Mandrus, D. G.; Yao, W.; Xu, X. Valley-Polarized Exciton Dynamics in a 2D Semiconductor Heterostructure. *Science* **2016**, *351*, 688−691.

(22) Hanbicki, A. T.; Chuang, H.-J.; Rosenberger, M. R.; Hellberg, C. S.; Sivaram, S. V.; McCreary, K. M.; Mazin, I. I.; Jonker, B. T. Double Indirect Interlayer Exciton in a $MoSe_2/WSe_2$ van Der Waals Heterostructure. *ACS Nano* **2018**, *12*, 4719−4726.

(23) Gong, Y.; Lei, S.; Ye, G.; Li, B.; He, Y.; Keyshar, K.; Zhang, X.; Wang, Q.; Lou, J.; Liu, Z.; Vajtai, R.; Zhou, W.; Ajayan, P. M. Two-Step Growth of Two-Dimensional WSe_2 /$MoSe_2$ Heterostructures. *Nano Lett.* **2015**, *15*, 6135−6141.

(24) Solís-Fernández, P.; Bissett, M.; Ago, H. Synthesis, Structure and Applications of Graphene-Based 2D Heterostructures. *Chem. Soc. Rev.* **2017**, *46*, 4572−4613.

(25) Tongay, S.; Fan, W.; Kang, J.; Park, J.; Koldemir, U.; Suh, J.; Narang, D. S.; Liu, K.; Ji, J.; Li, J.; Sinclair, R.; Wu, J. Tuning Interlayer Coupling in Large-Area Heterostructures with CVD-Grown MoS_2 and WS_2 Monolayers. *Nano Lett.* **2014**, *14*, 3185−3190.

(26) Duan, X.; Wang, C.; Shaw, J. C.; Cheng, R.; Chen, Y.; Li, H.; Wu, X.; Tang, Y.; Zhang, Q.; Pan, A.; Jiang, J.; Yu, R.; Huang, Y.; Duan, X. Lateral Epitaxial Growth of Two-Dimensional Layered Semiconductor Heterojunctions. *Nat. Nanotechnol.* **2014**, *9*, 1024−1030.

(27) Das, S.; Gulotty, R.; Sumant, A. V.; Roelofs, A. All Two-Dimensional, Flexible, Transparent, and Thinnest Thin Film Transistor. *Nano Lett.* **2014**, *14*, 2861−2866.

(28) Deng, Y.; Luo, Z.; Conrad, N. J.; Liu, H.; Gong, Y.; Najmaei, S.; Ajayan, P. M.; Lou, J.; Xu, X.; Ye, P. D. Black Phosphorus−Monolayer MoS_2 van Der Waals Heterojunction p−n Diode. *ACS Nano* **2014**, *8*, 8292−8299.

(29) Walmsley, T. S.; Chamlagain, B.; Rijal, U.; Wang, T.; Zhou, Z.; Xu, Y. Gate-Tunable Photoresponse Time in Black Phosphorus−MoS_2 Heterojunctions. *Adv. Opt. Mater.* **2019**, *7*, 1800832.

(30) Chuang, H.-J.; Chamlagain, B.; Koehler, M.; Perera, M. M.; Yan, J.; Mandrus, D.; Tománek, D.; Zhou, Z. Low-Resistance 2D/2D Ohmic Contacts: A Universal Approach to High-Performance WSe_2 , MoS_2 , and $MoSe_2$ Transistors. *Nano Lett.* **2016**, *16*, 1896−1902.

(31) Long, M.; Wang, P.; Fang, H.; Hu, W. Progress, Challenges, and Opportunities for 2D Material Based Photodetectors. *Adv. Funct. Mater.* **2019**, 1−28.

(32) Chang, Y.-H.; Zhang, W.; Zhu, Y.; Han, Y.; Pu, J.; Chang, J.-K.; Hsu, W.-T.; Huang, J.-K.; Hsu, C.-L.; Chiu, M.-H.; Takenobu, T.; Li, H.; Wu, C.-I.; Chang, W.-H.; Wee, A. T. S.; Li, L.-J. Monolayer $MoSe_2$ Grown by Chemical Vapor Deposition for Fast Photodetection. *ACS Nano* **2014**, *8*, 8582−8590.
(33) Tongay, S.; Zhou, J.; Ataca, C.; Lo, K.; Matthews, T. S.; Li, J.; Grossman, J. C.; Wu, J. Thermally Driven Crossover from Indirect toward Direct Bandgap in 2D Semiconductors: $MoSe_2$ versus MoS_2. *Nano Lett.* **2012**, *12*, 5576−5580.
(34) Zhang, Y.; Chang, T.-R.; Zhou, B.; Cui, Y.-T.; Yan, H.; Liu, Z.; Schmitt, F.; Lee, J.; Moore, R.; Chen, Y.; Lin, H.; Jeng, H.-T.; Mo, S.-K.; Hussain, Z.; Bansil, A.; Shen, Z.-X. Direct Observation of the Transition from Indirect to Direct Bandgap in Atomically Thin Epitaxial $MoSe_2$. *Nat. Nanotechnol.* **2014**, *9*, 111−115.
(35) Lee, H.; Ahn, J.; Im, S.; Kim, J.; Choi, W. High-Responsivity Multilayer $MoSe_2$ Phototransistors with Fast Response Time. *Sci. Rep.* **2018**, *8*, 11545.
(36) Mao, J.; Yu, Y.; Wang, L.; Zhang, X.; Wang, Y.; Shao, Z.; Jie, J. Ultrafast, Broadband Photodetector Based on $MoSe_2$ /Silicon Heterojunction with Vertically Standing Layered Structure Using Graphene as Transparent Electrode. *Adv. Sci.* **2016**, *3*, 1600018.
(37) Abderrahmane, A.; Ko, P. J.; Thu, T. V.; Ishizawa, S.; Takamura, T.; Sandhu, A. High Photosensitivity Few-Layered $MoSe_2$ Back-Gated Field-Effect Phototransistors. *Nanotechnology* **2014**, *25*, 365202.
(38) Jung, C.; Kim, S. M.; Moon, H.; Han, G.; Kwon, J.; Hong, Y. K.; Omkaram, I.; Yoon, Y.; Kim, S.; Park, J. Highly Crystalline CVD-Grown Multilayer $MoSe_2$ Thin Film Transistor for Fast Photodetector. *Sci. Rep.* **2015**, *5*, 15313.
(39) Rivera, P.; Schaibley, J. R.; Jones, A. M.; Ross, J. S.; Wu, S.; Aivazian, G.; Klement, P.; Seyler, K.; Clark, G.; Ghimire, N. J.; Yan, J.; Mandrus, D. G.; Yao, W.; Xu, X. Observation of Long-Lived Interlayer Excitons in Monolayer $MoSe_2$−WSe_2 Heterostructures. *Nat. Commun.* **2015**, *6*, 6242.
(40) Hamamatsu. Si Photodiodes E. 2014, No. February, 1−6.
(41) Dean, C. R.; Young, A. F.; Meric, I.; Lee, C.; Wang, L.; Sorgenfrei, S.; Watanabe, K.; Taniguchi, T.; Kim, P.; Shepard, K. L.; Hone, J. Boron Nitride Substrates for High-Quality Graphene Electronics. *Nat. Nanotechnol.* **2010**, *5*, 722−726.
(42) Larentis, S.; Fallahazad, B.; Tutuc, E. Field-Effect Transistors and Intrinsic Mobility in Ultra-Thin $MoSe_2$ Layers. *Appl. Phys. Lett.* **2012**, *101*, 223104.
(43) Chamlagain, B.; Li, Q.; Ghimire, N. J.; Chuang, H.-J.; Perera, M. M.; Tu, H.; Xu, Y.; Pan, M.; Xaio, D.; Yan, J.; Mandrus, D.; Zhou, Z. Mobility Improvement and Temperature Dependence in $MoSe_2$ Field-Effect Transistors on Parylene-C Substrate. *ACS Nano* **2014**, *8*, 5079−5088.
(44) Rhyee, J.-S.; Kwon, J.; Dak, P.; Kim, J. H.; Kim, S. M.; Park, J.; Hong, Y. K.; Song, W. G.; Omkaram, I.; Alam, M. A.; Kim, S. High-Mobility Transistors Based on Large-Area and Highly Crystalline CVD-Grown $MoSe_2$ Films on Insulating Substrates. *Adv. Mater.* **2016**, *28*, 2316−2321.
(45) Wang, T.; Andrews, K.; Bowman, A.; Hong, T.; Koehler, M.; Yan, J.; Mandrus, D.; Zhou, Z.; Xu, Y.-Q. High-Performance WSe_2 Phototransistors with 2D/2D Ohmic Contacts. *Nano Lett.* **2018**, *18*, 2766−2771.
(46) Quereda, J.; Ghiasi, T. S.; van Zwol, F. A.; van der Wal, C. H.; van Wees, B. J. Observation of Bright and Dark Exciton Transitions in Monolayer $MoSe_2$ by Photocurrent Spectroscopy. *2D Mater.* **2017**, *5*, No. 015004.
(47) He, K.; Kumar, N.; Zhao, L.; Wang, Z.; Mak, K. F.; Zhao, H.; Shan, J. Tightly Bound Excitons in Monolayer WSe_2. *Phys. Rev. Lett.* **2014**, *113*, No. 026803.
(48) Wang, G.; Gerber, I. C.; Bouet, L.; Lagarde, D.; Balocchi, A.; Vidal, M.; Amand, T.; Marie, X.; Urbaszek, B. Exciton States in Monolayer $MoSe_2$: Impact on Interband Transitions. *2D Mater.* **2015**, *2*, No. 045005.
(49) Arora, A.; Nogajewski, K.; Molas, M.; Koperski, M.; Potemski, M. Exciton Band Structure in Layered $MoSe_2$: From a Monolayer to the Bulk Limit. *Nanoscale* **2015**, *7*, 20769−20775.
(50) Kumar, A.; Ahluwalia, P. K. Electronic Structure of Transition Metal Dichalcogenides Monolayers 1H-MX_2 (M = Mo, W; X = S, Se, Te) from Ab-Initio Theory: New Direct Band Gap Semiconductors. *Eur. Phys. J. B* **2012**, *85*, 186.
(51) Mak, K. F.; Lee, C.; Hone, J.; Shan, J.; Heinz, T. F. Atomically Thin MoS_2: A New Direct-Gap Semiconductor. *Phys. Rev. Lett.* **2010**, *105*, 136805.
(52) Wang, B.; Yang, S.; Wang, C.; Wu, M.; Huang, L.; Liu, Q.; Jiang, C. Enhanced Current Rectification and Self-Powered Photoresponse in Multilayer p-$MoTe_2$/n-MoS_2 van Der Waals Heterojunctions. *Nanoscale* **2017**, *9*, 10733−10740.
(53) Perea-López, N.; Elías, A. L.; Berkdemir, A.; Castro-Beltran, A.; Gutiérrez, H. R.; Feng, S.; Lv, R.; Hayashi, T.; López-Urías, F.; Ghosh, S.; Muchharla, B.; Talapatra, S.; Terrones, H.; Terrones, M. Photosensor Device Based on Few-Layered WS_2 Films. *Adv. Funct. Mater.* **2013**, *23*, 5511−5517.
(54) Groenendijk, D. J.; Buscema, M.; Steele, G. A.; Michaelis de Vasconcellos, S.; Bratschitsch, R.; van der Zant, H. S. J.; Castellanos-Gomez, A. Photovoltaic and Photothermoelectric Effect in a Double-Gated WSe_2 Device. *Nano Lett.* **2014**, *14*, 5846−5852.
(55) Tang, W.; Liu, C.; Wang, L.; Chen, X.; Luo, M.; Guo, W.; Wang, S.-W.; Lu, W. MoS_2 Nanosheet Photodetectors with Ultrafast Response. *Appl. Phys. Lett.* **2017**, *111*, 153502.
(56) Qin, J.-K.; Ren, D.-D.; Shao, W.-Z.; Li, Y.; Miao, P.; Sun, Z.-Y.; Hu, P.; Zhen, L.; Xu, C.-Y. Photoresponse Enhancement in Monolayer ReS_2 Phototransistor Decorated with CdSe−CdS−ZnS Quantum Dots. *ACS Appl. Mater. Interfaces* **2017**, *9*, 39456−39463.
(57) Moun, M.; Singh, A.; Tak, B. R.; Singh, R. Study of the Photoresponse Behavior of a High Barrier Pd/MoS_2/Pd Photodetector. *J. Phys. D: Appl. Phys.* **2019**, *52*, 325102.
(58) Pradhan, N. R.; Ludwig, J.; Lu, Z.; Rhodes, D.; Bishop, M. M.; Thirunavukkuarasu, K.; McGill, S. A.; Smirnov, D.; Balicas, L. High Photoresponsivity and Short Photoresponse Times in Few-Layered WSe_2 Transistors. *ACS Appl. Mater. Interfaces* **2015**, *7*, 12080−12088.
(59) Zhang, W.; Huang, J.-K.; Chen, C.-H.; Chang, Y.-H.; Cheng, Y.-J.; Li, L.-J. High-Gain Phototransistors Based on a CVD MoS_2 Monolayer. *Adv. Mater.* **2013**, *25*, 3456−3461.
(60) Wojtas, J.; Mikolajczyk, J.; Bielecki, Z. Aspects of the Application of Cavity Enhanced Spectroscopy to Nitrogen Oxides Detection. *Sensors* **2013**, *13*, 7570−7598.

https://dx.doi.org/10.1021/acsami.0c12155
ACS Appl. Mater. Interfaces 2020, 12, 46476−46482